Remote Sens. **2011**, *3*, 1535-1552; doi:10.3390/rs3071535

OPEN ACCESS

Remote Sensing

ISSN 2072-4292

www.mdpi.com/journal/remotesensing

Article

Urban Heat Island Analysis Using the Landsat TM Data and ASTER Data: A Case Study in Hong Kong

Lin Liu and Yuanzhi Zhang *

Institute of Space and Earth Information Science, Yuen Yuen Research Centre for Satellite Remote Sensing, The Chinese University of Hong Kong, Shatin, Hong Kong, China;
E-Mail: niceliulin@126.com

* Author to whom correspondence should be addressed; E-Mail: yuanzhizhang@cuhk.edu.hk; Tel.: +852-3163-4409; Fax: +852-2603-7470.

Received: 21 May 2011; in revised form: 28 May 2011 / Accepted: 4 July 2011 / Published: 13 July 2011

Abstract: In this paper, the effect of urban heat island is analyzed using the Landsat TM data and ASTER data in 2005 as a case study in Hong Kong. Two algorithms were applied to retrieve the land surface temperature (LST) distribution from the Landsat TM and ASTER data. The spatial pattern of LST in the study area is retrieved to characterize their local effects on urban heat island. In addition, the correlation between LST and the normalized difference vegetation index (NDVI), the normalized difference build-up index (NDBI) is analyzed to explore the impacts of the green land and the build-up land on the urban heat island by calculating the ecological evaluation index of sub-urban areas. The results indicate that the effect of urban heat island in Hong Kong is mainly located in three sub-urban areas, namely, Kowloon Island, the northern Hong Kong Island and Hong Kong International Airport. The correlation between LST and NDVI, NDBI also indicates that the negative correlation of LST and NDVI suggests that the green land can weaken the effect on urban heat island, while the positive correlation between LST and NDBI means that the built-up land can strengthen the effect of urban heat island in our case study. Although satellite data (e.g., Landsat TM and ASTER thermal bands data) can be applied to examine the distribution of urban heat islands in places such as Hong Kong, the method still needs to be refined with *in situ* measurements of LST in future studies.

Keywords: Landsat TM; ASTER; land surface temperature; urban heat island; Hong Kong

---

1. Introduction

It is well known and documented that urbanization can have significant effects on local weather and climate [1]. Of these effects one of the most familiar is the urban heat island [2], which is the direct representation of environmental degradation [3]. An urban heat island is a metropolitan area which is significantly warmer than its surrounding rural areas; the higher urbanization leads to more distinct urban heat island with huge temperature differences between urban and rural areas. As early as 1833, the concept of urban heat island was described by Luke Howard [4], and since then this research topic has received ever more attention [5-13]. Recently, with the development of society and acceleration of the process of urbanization, the urban heat island has become more and more significant and has had severe impact on urban development and human living environments [14]. The buildings, concrete, asphalt and industrial activity of urban areas causes the urban heat island. Replacing natural land cover with pavements, buildings and other infrastructures takes away the natural cooling effects. Also, tall buildings and narrow streets can heat the air trapped between them and reduce airflow. In addition, heat from vehicles, factories and air conditioners adds warmth to the surroundings, further exacerbating the heat island effect. Urban heat island can impact local weather and climate, altering local wind patterns, spurring the development of clouds and fog, increasing the number of lightning events, and influencing the rates of precipitation. Furthermore, the poor air quality that results from the increased energy usage for cooling purposes in heat-island city can cause discomfort for human beings and affect health, aggravating asthma and promoting other respiratory illnesses. Thus, it is practical and indispensable to do research on the analysis of urban heat island, which can provide information and advice for our future urban planning and environment protection.

Urban heat island mainly appeared in the spatial distribution of land surface temperature (LST), which is governed by surface heat fluxes and obviously affected by urbanization [15,16]. Consequently, acquiring LST is the primary and key step to the urban heat island analysis. The LST difference is usually larger at night than during the day. Seasons influence the LST difference, too. Heat island cities located in the mid latitude usually are strongest in the summer seasons. In tropical climates, the day season may affect the large island magnitudes. Thus, there are differences in day, night and seasonal measurements of LST. So when the land surface temperature is unavailable in the case studies, the near-surface air temperature can also be used to validate the urban heat island effect. Traditionally, urban heat island analysis is based on the LST data observed at the meteorological points always with *in situ* measurements [3]. However, the uneven distribution and limited conditions of these isolated meteorological observation locations may result in the observed LST data not fully representing the distribution of LST across the region. Since the 1960s, with the advent of high-resolution earth-monitoring satellites, remote sensing technology has been widely utilized to measure LST and provide basic data for the urban heat island analysis. Compared to the traditional meteorological observation method, remote sensing technology has the advantages of high-resolution, wide-coverage and intensive-points, *etc*., which makes large-scale urban heat island research possible.

The Landsat TM data is one of the most widely used satellite images for LST retrieving because of its high resolution (120 m) and free download availability from the website of US Geological Survey (USGS), which has one thermal infrared (TIR) band. This makes retrieving LST from a single band more difficult than from multiple thermal bands. In 2001, Qin *et al.* proposed a mono-window

algorithm for retrieving LST using Landsat TM TIR band data [17]. The mono-window algorithm provided a simple and highly effective method for retrieving land surface temperatures for the analysis of urban heat island effect [3]. In comparison, ASTER data has five thermal bands with a higher resolution (90 m), which may provide more promising potential for LST retrieval studies, although very few studies of LST retrieval from ASTER data are available as yet. Therefore, in this study, we applied the mono-window algorithm to the Landsat TM and the split-window algorithm to ASTER data for the analysis of its effect of urban heat island in the case study of Hong Kong. Although satellite data (e.g., Landsat TM and ASTER thermal bands data) can be applied to examine the distribution of urban heat islands in places such as Hong Kong, the method still needs to be refined with *in situ* measurements of LST in future studies.

2. Study Area and Data

2.1. Study Area

The study area of Hong Kong (between 22°9'14"N to 22°33'44"N and 113°50'7"E to 114°26'30"E) (Figure 1) is one of two special administrative regions of the People's Republic of China, the other being Macau. Located in the south-eastern tip of the mainland of China, with a total area of 1,104 square kilometers, it consists of Hong Kong Island, Kowloon Peninsula, New Territories, and over 200 offshore islands, of which the largest is Lantau Island. Of the total area, 1,054 km^2 is land and 50 km^2 is inland water. Situated just south of the Tropic of Cancer, Hong Kong's climate is humid sub-tropical, tending towards temperate for nearly half the year. Hong Kong averages 1,948 hours of sunshine per year, and about 90 percent of its rainfall occurs between April and September. Temperatures can drop below 10 °C in winter and exceed 31 °C in summer.

Figure 1. The study area of Hong Kong.

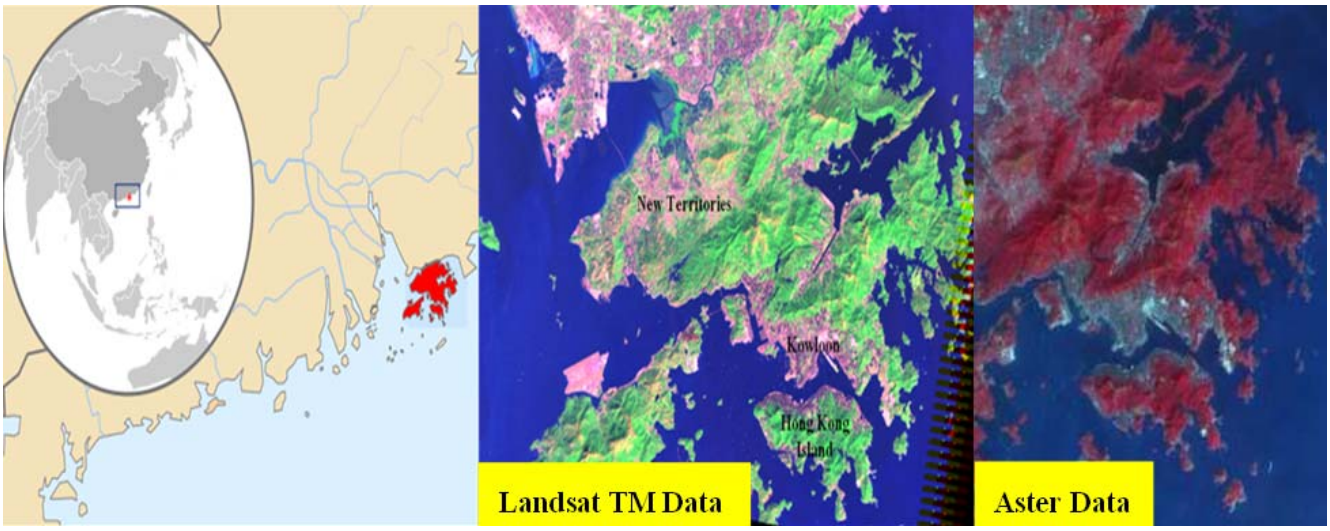

Hong Kong is one of the most densely populated areas in the world and the world's leading international financial center. The lack of available sprawl space caused the demand for denser constructions, which made Hong Kong become the world's most vertical city with expansive skyline. The intense urbanization and dense building finally result in the urban heat island effect with huge

temperature differences between urban and rural areas. The temperature variations may be attributable to greater absorbency of man-made materials, and denser buildings which restrict air-flow. It is very important to conduct an urban heat island analysis of Hong Kong and evaluate its impact on urban environment in the city.

2.2. Data

2.2.1. Satellite Image Data

In this study, the Landsat TM data and ASTER data (Table 1) are used for the analysis of urban heat island in Hong Kong.

Table 1. Landsat TM and ASTER satellite image data.

Data	Resolution (m)	Time	Date
Landsat TM	120 × 120	02:40	23 November 2005
ASTER L1A	90 × 90	03:08	1 December 2005

2.2.2. Other Auxiliary Data

In addition, the Hong Kong Topographic Map and Hong Kong Regional Map were used in the study. They are both available from Survey and Mapping Office and Land Department of Hong Kong.

2.2.3. Data Pre-Processing

The data pre-processing is performed using ERDAS Imagine 9.2 software.

Each TM/ETM file is composed of the independent single-band images. Thus, it is firstly used to combine the single-band images to a multi-bands image of TM/ETM using a layer stacking tool. Secondly, the geometric correction was made for the TM/ETM images, by which each point on the image would have only latitude or longitude geographical coordinates. This is the most important step in pre-processing. Thirdly, after geometric correction, the image subset tool was used to clip our study area. For the ASTER L1A data, the above second and third steps only were used. Figure 2 shows the basic procedures of the two satellite data pre-processing. After the pre-processing, the study area images of Hong Kong were obtained for the data processing and analysis of urban heat island.

Figure 2. The data pre-processing procedures.

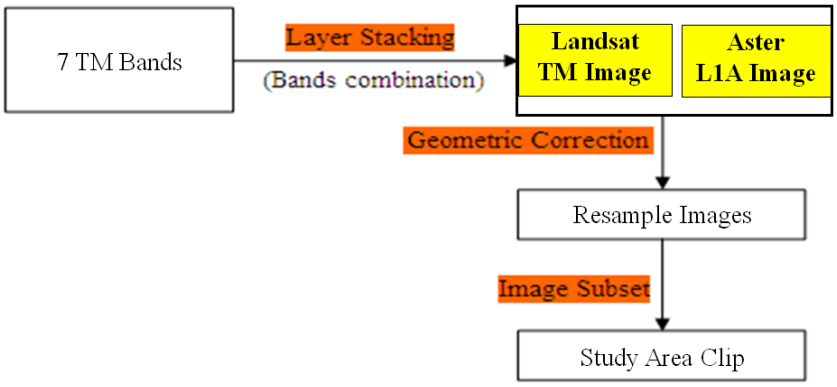

3. LST Retrieval Methodology

3.1. Brief Introduction to Different LST Retrieval Methods

Different LST retrieval methods have been developed according to different data sources, such as the split-window method [18], temperature/emissivity separation method [19], mono-window method [17], and the single-channel method [20].

With relative higher resolution and easy availability, Landsat satellite is one of the longest running programs for global change research and has been applied for agriculture, geology, regional planning and urban environment. As the thermal infrared (TIR) channel, band 6 records the radiation with spectral range in 10.4–12.5 μm from the surface of the earth. Three LST retrieval methods: radiative transfer equation, mono-window algorithm and single-channel algorithm can be applied to Landsat TM 6 data. Although all of these methods can provide good results, the radiative transfer equation is not available without *in situ* parameters of atmospheric profiles simultaneously when the satellite passes. The mono-window algorithm with radio sounding data can get a better result than the single-channel algorithm with a root mean square deviation of 0.9 K [21]. Unlike for Landsat TM data, all the above methods are feasible for ASTER data due to its multiple thermal bands.

Thus, the mono-window algorithm (Table 2) is applied in this study to retrieve the LST of Hong Kong from Landsat TM data and ASTER data.

Table 2. LST retrieval methods.

Algorithm / Data	Temperature/Emissivity Separation	Single-Channel	Mono-Window	Split-Window	Multi-Window
Landsat TM (1 thermal band)	√ (*in situ* parameters required)	√ (lower accuracy)	√ (higher accuracy)		
ASTER L1A (5 thermal bands)	√	√	√	√	√

3.2. Mono-Window Algorithm and Split-Window Algorithm

Urban heat island effect studies with LST derived from Landsat TM 6 data have been widely conducted. In 2001, Qin *et al.* proposed the mono-window algorithm (Figure 3) for retrieving LST from Landsat TM 6 data [17]. Based on thermal radiance transfer equation, the mono-window algorithm only requires three parameters—emissivity, transmittance and effective mean atmospheric temperature—to retrieve LST from Landsat TM 6. Band 6 records the radiation with spectral range in 10.4–12.5 μm. Similarly, ASTER band 13 is 10.25–10.95 μm and ASTER band 14 is 10.95–11.65 μm. In this study, the mono-window algorithm is used for Landsat TM 6, while the split-window algorithm is applied for ASTER 13 and ASTER 14 in the case study of Hong Kong.

Figure 3. The flowchart of the mono-window algorithm.

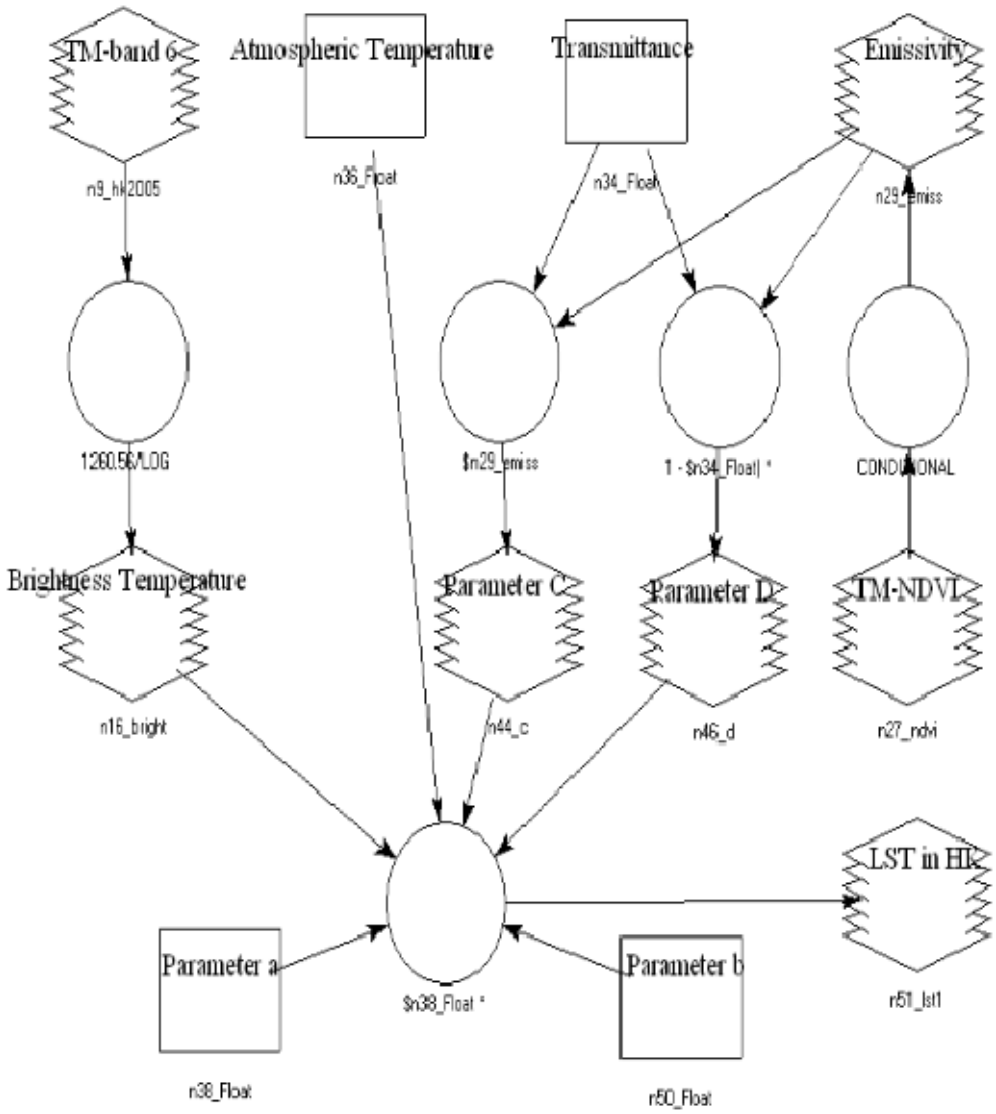

As one of the most widely used software packages in the field of satellite image processing, the spatial modeler module in ERDAS imagine software provides a powerful tool to accomplish most image processing functions [16]. The spatial model to retrieve LST from Landsat TM and ASTER data using ERDAS spatial model tool is designed. In this model, only two measured parameters are required; near-surface air temperature and water vapor content simultaneously when satellite passes, which can be easily obtained from local weather stations. These two parameters are then converted to air transmittance and effective mean atmospheric temperature. The third required parameter is the emissivity, which can be calculated from the normalized difference vegetation index (NDVI). The remaining useful values can all be obtained from the Meta file in the satellite image data.

(1) Convert the digital number (DN) into spectral radiance:

In order to convert the DN data (from Landsat TM 6, ASTER 13 and ASTER 14) into spectral radiance, Equation (1) [17] can be written as:

$$L_i = L_{min} + (L_{max} - L_{min}) Q_{dn} / Q_{max} \quad (1)$$

where L_i is the at-sensor spectral radiance ($MW \cdot cm^{-2} \cdot sr^{-1} \cdot \mu m^{-1}$); L_{max} is the maximum at-sensor spectral radiance; L_{min} is the minimum at-sensor spectral radiance; Q_{max} represents the maximum DN value of pixels and Q_{dn} represents the DN value of pixel.

For Landsat TM 6 data, Equation 1 can be expressed as Equation (2):

$$L_6 = 0.005\,632\,156\,Q_{dn} + 0.123\,8 \tag{2}$$

where L_6 is the at-sensor spectral radiance of Landsat TM 6, and Q_{dn} is the DN value of pixel.

For ASTER 13 data, Equation (1) can be written as Equation (3):

$$L_{13} = 0.005693 Q_{dn} - 0.005693 \tag{3}$$

where L_{13} is the at-sensor spectral radiance of ASTER 13 and Q_{dn} represents the DN value of pixel.

For ASTER 14 data, Equation (1) can be expressed as Equation (4):

$$L14 = 0.005225\ Q_{dn} - 0.005225 \tag{4}$$

where L_{14} is the at-sensor spectral radiance of ASTER 14 and Q_{dn} represents the DN value of pixel.

(2) Convert the spectral radiance into at-sensor brightness temperature:

In order to convert the spectral radiance into at-sensor brightness temperature, the Planck's function can be used as Equation (5) [17]:

$$T_i = C_2 / \{\lambda_i \times \ln[1 + C_1 / (\lambda_i^5 \times L_i)]\} \tag{5}$$

$$C_1 = 1.191\,043\,56 \times 10^{-16} W \cdot m^2 \tag{6}$$

$$C_2 = 1.438\,768\,5 \times 10^4\ \mu m \cdot K \tag{7}$$

where T_i is the at-sensor brightness temperature (K); C_2, C_1 are constants; λ_i is central wavelength and L_i represents the at-sensor spectral radiance, which can be calculated using Equation (1). For ASTER 13 data, λ_{13} = 10.6 μm. For ASTER 14 data, λ_{14} = 11.3 μm.

For Landsat TM 6 data, Equation (8) [17] can be used, in which the Planck's function is similar with the two free parameters of K_1 and K_2:

$$T_6 = K_2 / \ln(1 + K_1 / L_6) \tag{8}$$

$$K_1 = 60.776\ MW \cdot cm^{-2} \cdot sr^{-1} \cdot \mu m^{-1} \tag{9}$$

$$K_2 = 1\,260.56\ K \tag{10}$$

where T_6 is the at-sensor brightness temperature of Landsat TM 6; K_1, K_2 are calibration constants of Landsat TM and L_6 represents the at-sensor spectral radiance of Landsat TM 6.

(3) Calculation of land surface emissivity:

In fact, the emissivity can be estimated by utilizing NDVI [22,23].

(i) Precise calculation of NDVI

The normalized difference vegetation index (NDVI) is one of the most widely applied vegetation indices. Doing ration calculation between the near infrared (NIR) band and the red (R) band can

strengthen the vegetation information and the ratio is the main idea of NDVI [3]. In order to calculate the NDVI, Equation (11) can be used as:

$$\mathrm{NDVI} = \frac{\mathrm{NIR} - \mathrm{R}}{\mathrm{NIR} + \mathrm{R}} \tag{11}$$

(ii) Estimation of emissivity

The emissivity [22,23] can be calculated from NDVI.

When NDVI values range from 0.157 to 0.727, Van De Griend and Owe [22] gave an effective equation (Equation (12)) as follows:

$$\varepsilon_{\mathrm{i}} = 1.009\,4 + 0.004\,7\ln(\mathrm{NDVI}) \tag{12}$$

In 2006 Zhang [23] proposed a complete land surface emissivity estimation method using NDVI (Table 3).

Table 3. Estimation of emissivity using NDVI.

NDVI	Land surface emissivity (ε_{i})
NDVI < −0.185	0.995
−0.185 ≤ NDVI < 0.157	0.970
0.157 ≤ NDVI ≤ 0.727	1.009 4 + 0.047ln(NDVI)
NDVI > 0.727	0.990

(4) Calculation of atmospheric transmittance:

Actually, the atmospheric transmittance can be estimated by using water vapor [16,17].

(i) Calculation of water vapor content

In order to calculate the water vapor, Equation 13 [24,25] can be used as:

$$w_i = 0.098\,1 \times \left\{ 10 \times 0.610\,8 \times \exp\left[\frac{17.27 \times (T_0 - 273.15)}{237.3 + (T_0 - 273.15)} \right] \times \mathrm{RH} \right\} + 0.169\,7 \tag{13}$$

where w_i is the water vapor content (g/cm^2); T_0 is the near-surface air temperature in K and RH represents the relative humidity. The water vapor content, near-surface air temperature and relative humidity are all from Hong Kong Observatory. For the Landsat TM 6 data, they are the average values of a total of 29 stations around Hong Kong on 23 November 2005. For ASTER 13 and 14 data, they are the average values of the same 29 stations on 1 December 2005.

(ii) Estimation of atmospheric transmittance

For Landsat TM 6 data, Equation (14) can be applied from Table 4 [16,17] to calculate the atmospheric transmittance of Landsat TM 6.

$$\tau_6 = 1.031412 - 0.11536 \times w_6 \tag{14}$$

where τ_6 is the atmospheric transmittance of Landsat TM 6 and w_6 represents the water vapor content, which can be calculated using Equation (13).

Table 4. Estimation of atmospheric transmittance.

Profiles	Water vapor (w_6) (g/cm^2)	Transmittance estimation equation (τ_6)	Squared correction	Standard error
High air temperature	0.4–1.6	$0.974290-0.08007\,w_6$	0.99611	0.002368
	1.6–3.0	$1.031412-0.115\,36\,w_6$	0.99827	0.002539
Low air temperature	0.4–1.6	$0.982007-0.09611\,w_6$	0.99563	0.003340
	1.6–3.0	$1.053710-0.14142\,w_6$	0.99899	0.002375

For ASTER 13 data and ASTER 14 data, Equations (15) and (16) can be used to calculate the atmospheric transmittance [26] as follows:

$$\tau_{13} = 1.02 - 0.104 \times w_{13} \tag{15}$$

$$\tau_{14} = 1.04 - 0.133 \times w_{14} \tag{16}$$

(5) Calculation of mean atmospheric temperature:

The mean atmospheric temperature equation from Table 5 [16,17] can be applied to the calculation of the mean atmospheric temperature.

Table 5. Estimation of mean atmospheric temperature.

Area	Atmospheric temperature equation (T_a) (K)
For USA 1976	$25.9396 + 0.88045 \times T_0$
For tropical	$17.9769 + 0.91715 \times T_0$
For mid-latitude summer	$16.0110 + 0.92621 \times T_0$
For mid-latitude winter	$19.2704 + 0.91118 \times T_0$

According to the location of Hong Kong, Equation (17) can be used for the estimation of mean atmospheric temperature as below:

$$T_a = 17.9769 + 0.91715 * T_0 \tag{17}$$

where T_0 is the near-surface air temperature (K).

(6) LST retrievals of the two algorithms:

The mono-window algorithm can be written as Equation (18) [17]. Three variables (*i.e.*, emissivity, transmittance and effective mean atmospheric temperature) are required as below:

$$T_S = \{a(1-C-D) + [b(1-C-D) + C + D]T_i - DT_a\}/C \tag{18}$$

$$a = -67.355351 \tag{19}$$

$$b = 0.458606 \tag{20}$$

$$C = \varepsilon_i \times \tau_i \tag{21}$$

$$D = (1 - \tau_i)[1 + (1 - \varepsilon_i) \times \tau_i] \tag{22}$$

where T_s is the LST (K); T_i is the brightness temperature (K), which can be calculated using Equation (5); ε_i is the emissivity, which can be classified and computed by NDVI (Table 3); τ_i is the transmittance, which can be calculated from Equations (14–16), and T_a represents the effective mean

atmospheric temperature, which can be calculated using Equation (17).

The split-window algorithm can be written as Equation (23) [26]. As Mao *et al.* [26] proposed the LST retrieval method using ASTER 13 and ASTER 14 data, Equation (23) can be expressed as follows:

$$\mathrm{T_S} = \{[C_{14}(D_{13}+B_{13})]-[C_{13}(D_{14}+B_{14})]\}/(C_{14}A_{13}-C_{13}A_{14}) \tag{23}$$

$$\mathrm{A_{13}} = 0.145\,236\times\varepsilon_{13}\times\tau_{13} \tag{24}$$

$$\mathrm{B_{13}} = 0.145\,236\times\mathrm{T_{13}}+33.685\times\varepsilon_{13}\times\tau_{13}-33.685 \tag{25}$$

$$\mathrm{C_{13}} = (1-\tau_{13})\times[1+(1-\varepsilon_{13})\times\tau_{13}]\times 0.145\,236 \tag{26}$$

$$\mathrm{D_{13}} = (1-\tau_{13})\times[1+(1-\varepsilon_{13})\times\tau_{13}]\times 33.685 \tag{27}$$

$$\mathrm{A_{14}} = 0.132\,66\times\varepsilon_{14}\times\tau_{14} \tag{28}$$

$$\mathrm{B_{14}} = 0.132\,66\times\mathrm{T_{14}}+30.273\times\varepsilon_{14}\times\tau_{14}-30.273 \tag{29}$$

$$\mathrm{C_{14}} = (1-\tau_{14})\times[1+(1-\varepsilon_{14})\times\tau_{14}]\times 0.132\,66 \tag{30}$$

$$\mathrm{D_{14}} = (1-\tau_{14})\times[1+(1-\varepsilon_{14})\times\tau_{14}]\times 30.273 \tag{31}$$

Figure 4 shows the LST results of Hong Kong in 2005 (November and December) datasets using the mono-window algorithm and the split-window algorithm, respectively, in which the left figure is the result from TM data and the right figure is the result from ASTER data. Both of the final LST results were expressed as °C. Table 6 gives all the parameters required for the LST retrieval and spatial mapping in the study.

Figure 4. LST results for Hong Kong in 2005 from Landsat TM (left) and ASTER data (right).

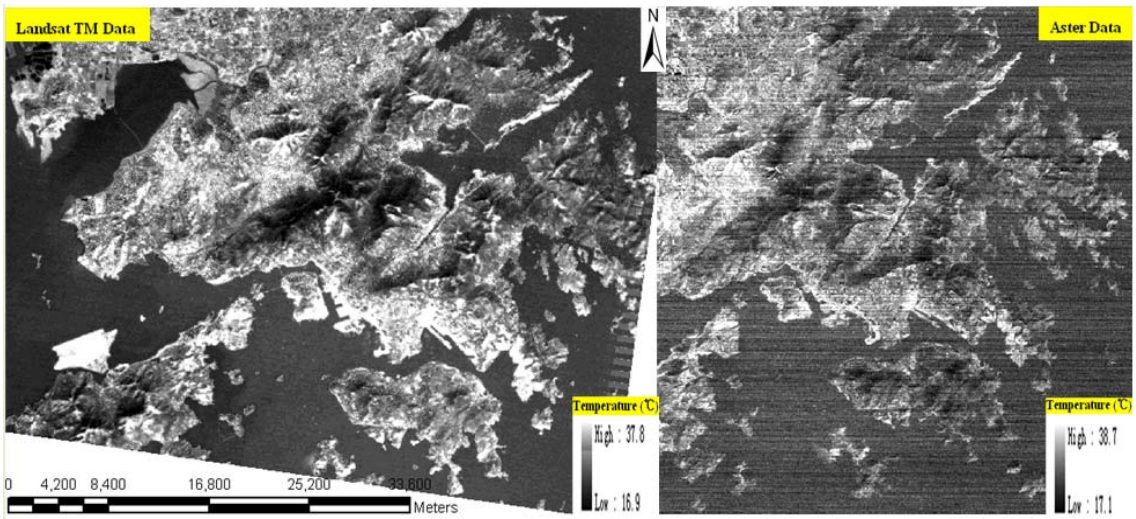

Table 6. All parameters used for retrieving LST for Hong Kong.

Parameters		Values			
Land surface emissivity	(ε_6)			NDVI	
	(ε_{13})	<−0.185	[−0.185,0.157]	[0.157,0.727]	>0.727
	(ε_{14})	0.995	0.970	1.0094 + 0.047ln(NDVI)	0.990
Atmospheric transmittance	(τ_6)			23 November 2005	
		T_0		RH	w_6
		20.9 °C		65%	1.75 g/cm^2
				0.83	
	(τ_{13})			1 December 2005	
		T_0		RH	w_{13}
		21.1 °C		79%	2.11 g/cm^2
				0.80	
	(τ_{14})			1 December 2005	
		T_0		RH	w_{14}
		21.1 °C		79%	2.11 g/cm^2
				0.76	
Mean atmospheric temperature	(T_a)			23 November 2005	
				T_0	
				20.9 °C	
				14.5 °C	
	(T_b)			1 December 2005	
				T_0	
				21.1 °C	
				14.7 °C	

4. Results and Discussion

4.1. The Accuracy Verification of LST Retrieval

In this study, the mean near-surface air temperature was used to verify the final retrieved LST results, due to the lack of simultaneous land surface temperature data when the satellite passes.

For the Landsat TM data, the mean temperature of retrieved LST is 294.72 K (or 21.6 °C) and the mean near-surface air temperature on 23 November 2005 is 294.05 K (or 20.9 °C). The LST retrieving error is about 0.7 K (or °C). Thus, the mono-window retrieving method from Landsat TM data has a better accuracy, which can provide high-quality retrieved LST data for the analysis of urban heat island.

For the ASTER data, the mean temperature of retrieved LST is 295.08 K (or 21.9 °C) and the mean near-surface air temperature on 1 December 2005 is 294.25 K (or 21.1 °C). The LST retrieving error is about 0.8 K (or °C). Furthermore, three representative areas and six points can be identified in Figure 5, in which the temperatures of these three representative areas are higher than other areas in both of the

LST retrieving results. Although the temperatures of the six points were not the same, their change trend is very close in Figure 6. The spatial consistency of the Landsat TM retrieving result [3] with an error of (0.7 K (or °C)) and the ASTER retrieving result [27] with an error of (0.8 K (or °C)) indicated that the two algorithms are comparable to the LST retrievals in the case study of Hong Kong. However, the comparison of the two algorithms should be investigated with more data collection in the near future.

Figure 5. The representative points and areas of two LST retrieving results.

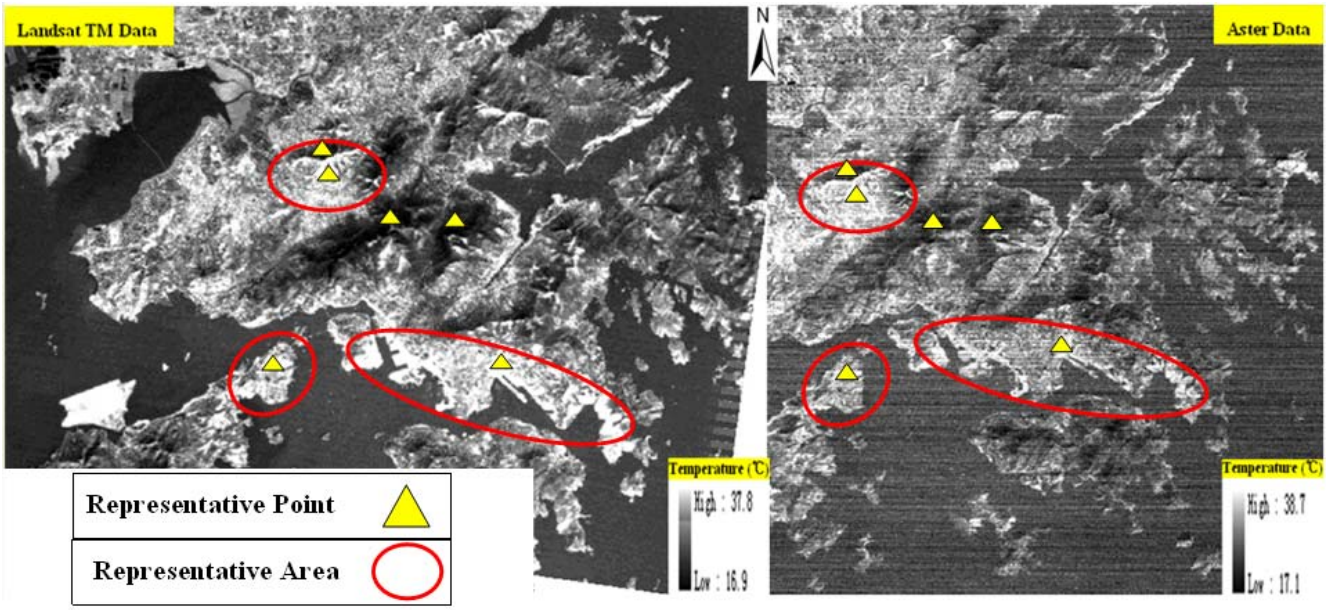

Figure 6. The retrieved LST variation curve of six representative points.

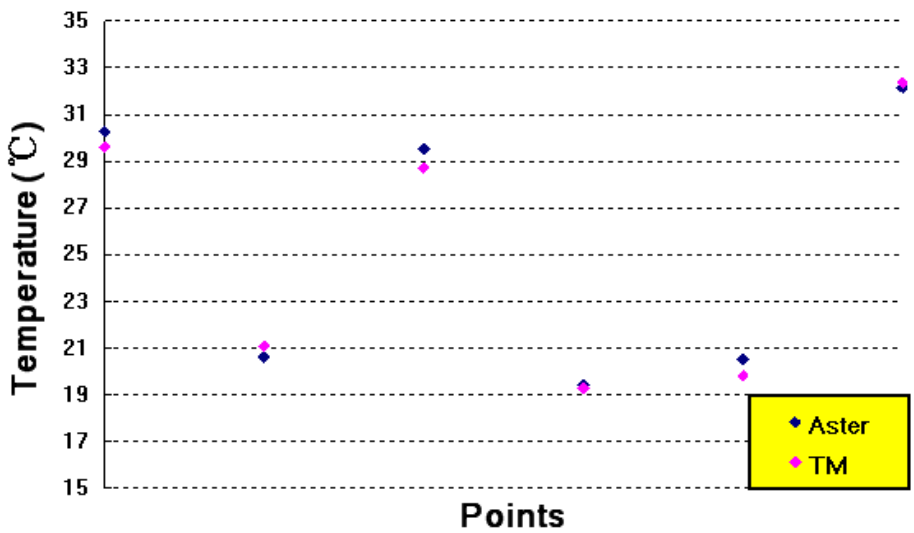

4.2. The Distribution of Urban Heat Islands in Hong Kong

From Figure 7, it is clear that severe urban heat island effects exist in Hong Kong. These urban heat islands are mainly distributed in several sub-urban areas such as the commercial centers in Kowloon Peninsula, the northern Hong Kong Island and Hong Kong International Airport.

Figure 7. The LST distribution in Hong Kong in 2005.

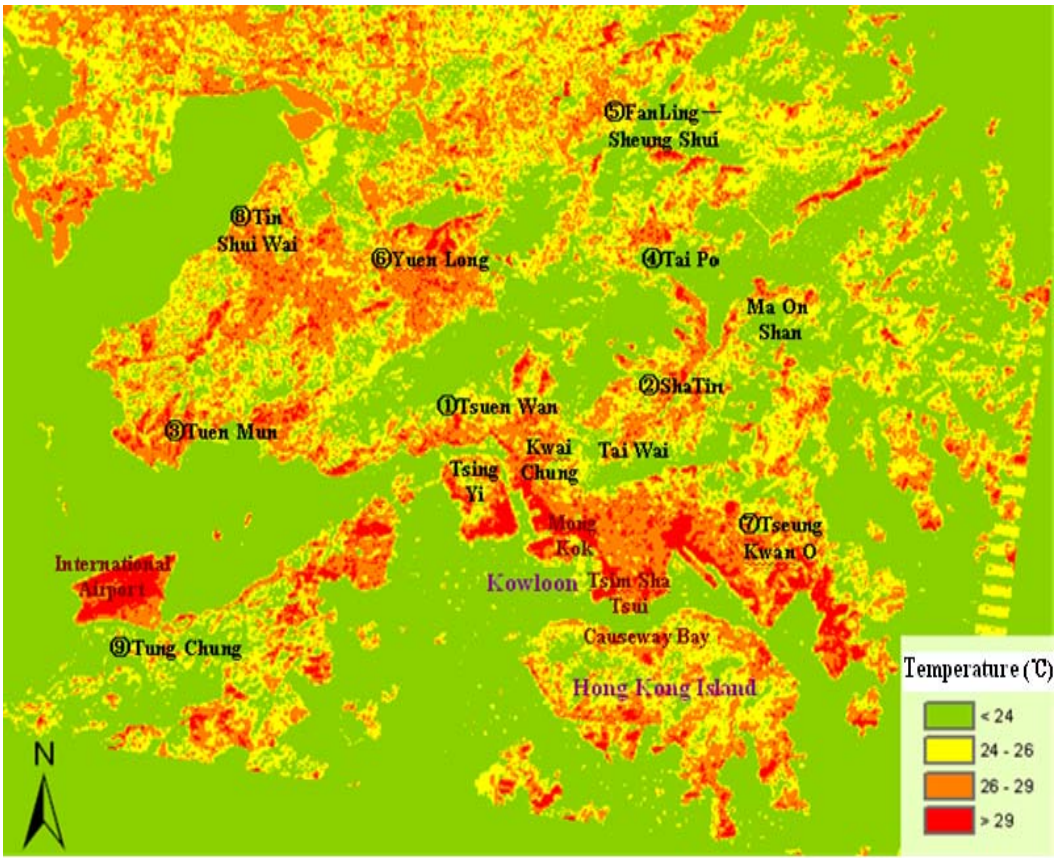

The temperature in the business centers in Kowloon and the northern Hong Kong Island (e.g., Mong Kok, Tsim Sha Tsui and Causeway Bay, *etc*.) was above 29 °C and the temperature of Chek Lap Kok (namely, Hong Kong International Airport) was also over 29 °C. These sub-urban areas show the strongest urban heat island effect. More and more constructions have been structured in Chek Lap Kok after the Hong Kong International Airport replaced the overcrowded Kai Tak Airport in Kowloon in 1998. Since both Kowloon and the North of Hong Kong Island are the business centers in Hong Kong, the high building density, property changes of underlying surface, air pollution and many artificial heat sources lead to the urban heat island effect in these sub-urban areas.

Even worse is that the distinct urban heat islands in Kowloon Peninsula have been converted into one large-scale regional heat island because of the tall buildings' dense distribution and expansion.

It is found that, the scattered settlements (satellite cities/new towns) throughout the New Territories in the northern Hong Kong also show to some extent heat island effect, but less intense than Kowloon, North of Hong Kong Island and Hong Kong International Airport. Figure 7 shows nine new sub-urban areas (or so-called satellite-cities) in Hong Kong: ① Tsuen Wan (Tsuen Wan, Kwai Chung and Tsing Yi included), 1973; ② Sha Tin (Sha Tin and Ma On Shan included), 1973; ③ Tuen Mun, 1973; ④ Tai Po, early 1980s; ⑤ Yuen Long, early 1980s; ⑥ Fanling-Sheung Shui, mid-1980s; ⑦ Tseung Kwan O, late 1980s; ⑧ Tin Shui Wai, early 1990s; ⑨ North Lantau (Tung Chung), 1997. The temperature of all nine places was between 26~29 °C, where residential construction is the dominant factor.

It is also noted that, because of the scattered distribution of the nine satellite-cities/new towns, their effects of urban heat islands distribute evenly, but do not as yet form a large-scale regional heat island like the Kowloon Peninsula.

Although satellite data (e.g., Landsat TM and ASTER thermal bands data) can be applied to examine the distribution of urban heat islands in places such as Hong Kong, the method for the calibration of LST still needs to be refined with *in situ* measurements of LST in future studies.

4.3. The Correlation Analysis between Urban Heat Island, NDVI and NDBI

NDVI (Normalized Difference Vegetation Index) is one of the most widely applied vegetation indices to strengthen the vegetation information [3]. In comparison, NDBI (Normalized Difference Build-up Index) is one of several widely used indices to strengthen building information and extract the built-up land from urban areas [3]. Because NDBI is the reflectivity of urban building and is higher in the fifth band than the fourth band, it can be calculated by using Equation (32) as follows:

$$\mathrm{NDBI} = \frac{\mathrm{MIR - NIR}}{\mathrm{MIR + NIR}} \tag{32}$$

In order to compare the green land and build-up land to urban heat island effects which provides useful information for the urban development and environment protection, the correlation between LST and NDVI, NDBI is analyzed. Table 7 shows their correlation coefficients. The correlation coefficient of LST and NDVI is −0.41, while the coefficient of LST and NDBI is 0.71. The negative coefficient between LST and NDVI indicates that the impact of green land on urban heat island is negative, which means that the green land can weaken the urban heat island effect. In comparison, the positive correlation between LST and NDBI suggests that the build-up land can strengthen the urban heat island effect in this case study.

Table 7. The correlation coefficient.

	LST	**NDVI**	**NDBI**
LST	1		
NDVI	−0.41	1	
NDBI	0.71	−0.56	1

4.4. The Ecological Valuation of Hong Kong Urban Heat Island

Urban thermal field variance index (UTFVI) was used to quantitatively describe the urban heat island effect [28]. UTFVI can be calculated using Equation (33) as below:

$$\mathrm{UTFVI} = \frac{T_S}{T_S - T_{MEAN}} \tag{33}$$

where UTFVI is the urban thermal field variance index; T_S is the LST of certain point in K and T_{MEAN} is the mean LST temperature of the whole study area in K.

To reflect the changes of urban thermal field directly, UTFVI can be further divided into six levels in accordance with six different ecological evaluation indices [28]. Table 8 gives the specific

thresholds in the six UTFVI levels and Figure 8 shows the ecological evaluation index of the case study in Hong Kong.

Table 8. The threshold of ecological evaluation index.

Urban thermal field variance index	Urban heat island phenomenon	Ecological evaluation index
<0	None	Excellent
0.000–0.005	Weak	Good
0.005–0.010	Middle	Normal
0.015–0.015	Strong	Bad
0.015–0.020	Stronger	Worse
>0.020	Strongest	Worst

Figure 8. The UTFVI classification map of ecological evaluation in Hong Kong.

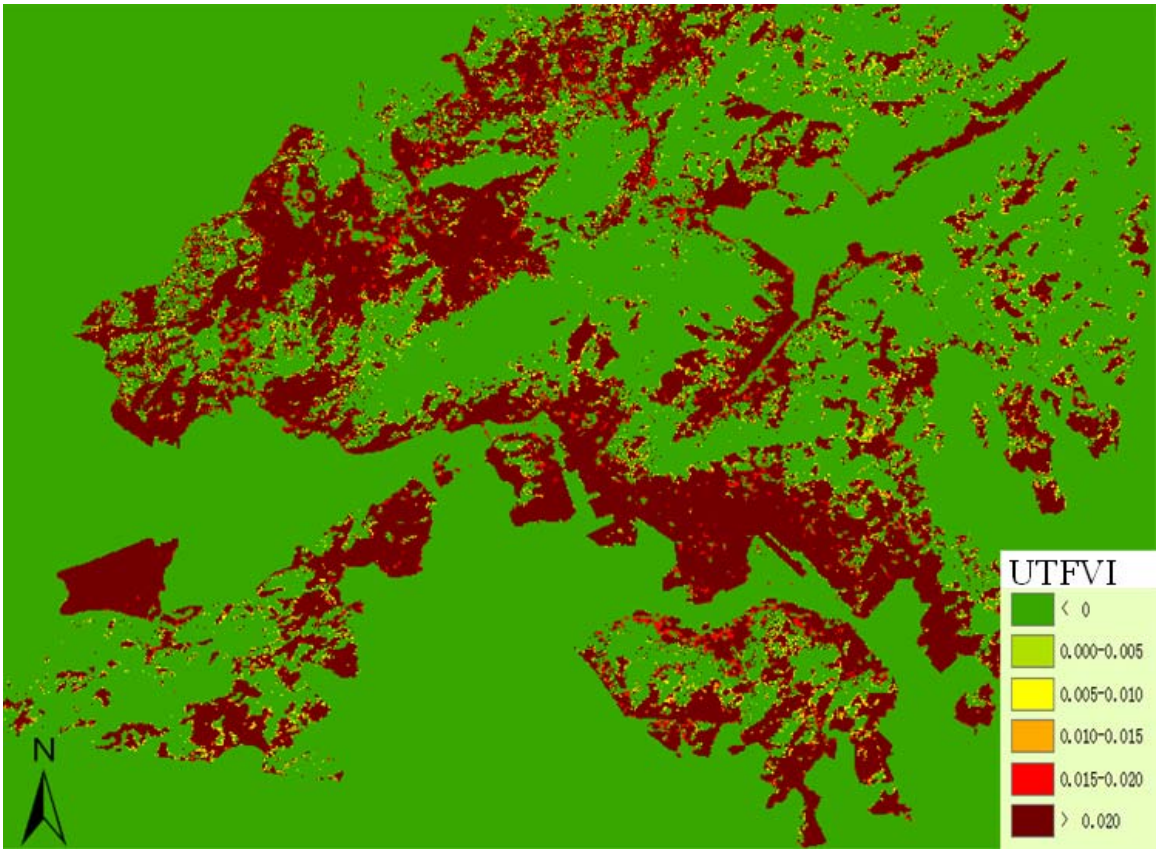

As much of Hong Kong's terrain is hilly to mountainous with steep slopes, less than 25% of the territory's landmass is developed. Most of the remaining undeveloped lands are either hills or reserved as country parks and nature reserves. These undeveloped areas all have high green vegetation coverage and excellent ecological evaluation index. Due to the limited land development of Hong Kong, most of the urban development exists on Kowloon Peninsula, along the northern edge of Hong Kong Island, and in scattered settlements throughout the New Territories. The concentrated urban development leads to the degraded eco-environment in these built-up areas with the worst ecological evaluation index.

From Figure 8, it is clear that two extreme levels have appeared in the ecological evaluation of Hong Kong: the excellent (<0) and the worst (>0.020). The UTFVI classification map of ecological evaluation in Hong Kong can also provide useful information for urban environment managers to evaluate eco-environmental quality. The severe urban heat island phenomenon calls for a more reasonable city layout and urban development to protect such an eco-environment in the future urban plan of Hong Kong as is achieved in other similar cities.

5. Conclusion

In this study, the mono-window algorithm and the split-window algorithm were applied to retrieve the land surface temperatures in Hong Kong using the Landsat TM data and ASTER data. Through the retrieved temperature data, it is found that the distribution of urban heat islands in Hong Kong is mainly located in Kowloon, the northern Hong Kong Island and Hong Kong International Airport.

In the Kowloon area, the urban heat islands have even conglomerated into one large-scale regional heat island because of the connected pieces of urban constructions. In comparison, the nine scattered satellite-cities have a dispersed distribution of urban heat island effects. So it is reasonable to envisage the establishment of satellite-cities in the city layout seperate from the business center in order to prevent the formation of a large-scale regional urban heat island. Although satellite data (e.g., Landsat TM and ASTER thermal bands data) can be applied to examine the distribution of urban heat islands in such cities as Hong Kong, the method still needs to be refined with *in situ* measurements of LST in future studies.

In addition, from the correlation analysis of the retrieved LST with NDVI and NBVI, it was found that that the green land can weaken urban heat island effect, but the built-up land can accelerate the effect. Thus, we have learnt that in the future city planning and development that more attention should be paid to urban greening.

Furthermore, from the ecological evaluation index calculation using UTFVI classification, it is noted that Hong Kong has strongest urban heat island phenomenon and worst eco-environment, which strongly calls for more reasonable city layout and urban development in the future.

However, the shortcoming in this case study is that the near surface air temperature data was used to assess the retrieving LST accuracy due to the lack of *in situ* LST data simultaneously available when the satellites passed. In future studies, the *in situ* LST data will be measured with the same overpass of satellites for the calibration and validation of the LST distribution as in the application and comparison of the two algorithms to be refined in Hong Kong and other similar urban areas.

Acknowledgements

The Landsat TM and ASTER data from US Geological Survey (USGS), the topographic map and regional map data from Hong Kong Survey and Mapping Office and Land Department, and near surface air temperature data from Hong Kong Observatory are highly appreciated in this research. The authors are extremely grateful to the Guest Editor, Thomas Blaschke and three anonymous reviewers to give helpful and critical comments to improve the original manuscript. The research is jointly supported by the CUHK Direct Grants, GRF (CUHK454909 and CUHK459210), and ITF (ITS/058/09FP).

References

1. Landsberg, H.E. *The Urban Climate*; Academic Press: New York, NY, USA, 1981; pp. 84-89.
2. Streutker, D.R. A remote sensing study of the urban heat island of Houston, Texas. *Int. J. Remote Sens.* **2002**, *23*, 2595-2608.
3. Lu, Y.; Feng, P.; Shen, C.; Sun, J. Urban Heat Island in Summer of Nanjing Based on TM Data. In *Proceedings of 2009 Joint Urban Remote Sensing Event*, Shanghai, China, 20–22 May 2009; pp. 1-5.
4. Howard, L. *The Climate of London*; London Harvey and Dorton: London, UK, 1833; Volume 2, pp. 1818-1820.
5. Detwiller, J. Deep soil temperature trends and urban effects at Paris. *J. Appl. Meteorol.* **1970**, *9*, 178-180.
6. Fukui, E. The recent rise of temperature in Japan. In *Japanese Progress in Climatology*; Tokyo University of Education: Tokyo, Japan, 1970; pp. 46-65.
7. Katsoulis, B.D.; Theoharatos, G.A. Indications of the urban heat island in Athens, Greece. *J. Clim. Appl. Meteorol.* **1985**, *24*, 1296-1302.
8. Wang, W.; Zheng, Z.; Karl, T.R. Urban Heat Islands in China. *Geophys. Res. Lett.* **1990**, *17*, 2377-2380.
9. Kim, H.H. Urban Heat Island. *Int. J. Remote Sens.* **1992**, *13*, 2319-2336.
10. Lee, H. An application of NOAA AVHRR thermal data to the study of urban heat Islands. *Atmos. Environ.* **1993**, *27*, 1-13.
11. Johnson, G.L.; Davis, J.M.; Karl, T.R.; McNab, A.L.; Gallo, K.P.; Tarpley, J.D.; Bloomfield, P. Estimating urban temperature bias using polar-orbiting satellite data. *J. Appl. Meteorol.* **1994**, *33*, 358-369.
12. Tso, C.P. A survey of urban heat island studies in two tropical cities. *Atmos. Environ.* **1996**, *30*, 507-519.
13. Camilloni, I.; Barros, V. On the urban heat island effect dependence on temperature trends. *Clim. Change* **1997**, *37*, 665-681.
14. Chen, Q; Ren, J.; Li, Z.; Ni, C. Urban Heat Island Effect Research in Chengdu City Based on MODIS Data. In *Proceedings of 3rd International Conference on Bioinformatics and Biomedical Engineering, ICBBE 2009*, Beijing, China, 11–13 June 2009; pp. 1-5.
15. Dousset, B.; Gourmelon, F. Satellite multi-sensor data analysis of urban surface temperatures and landcover. *ISPRS J. Photogram. Remote Sens.* **2003**, *58*, 43-54.
16. Sun, Q.; Tan, J.; Xu, Y. An ERDAS image processing method for retrieving LST and describing urban heat evolution: A case study in the Pearl River Delta Region in South China. *Environ. Earth Sci.* **2010**, *59*, 1047-1055.
17. Qin, Z.; Zhang, M.; Amon, K; Pedro, B. Mono-window Algorithm for retrieving land surface temperature from Landsat TM 6 data. *Acta Geogr. Sinica* **2001**, *56*, 456-466.
18. Sobrino, J.A.; Li, Z.L.; Stoll, M.P.; Becker, F. Multi-channel and multi-angle algorithms for estimating sea and land surface temperature with ATSR data. *Int. J. Remote Sens.* **1996**, *17*, 2089-2114.

19. Gillespie, A.R.; Rokugawa, S.; Matsunaga, T.; Cothern, J.S.; Hook, S.J.; Kahle, A.B. A temperature and emissivity separation algorithm for advanced spaceborne thermal emission and reflection radiometer (ASTER) images. *IEEE Trans. Geosci. Remote Sens.* **1998**, *36*, 1113-1126.
20. Jimenez-Munoz, J.C.; Sobrino, J.A. A generalized single-channel method for retrieving land surface temperature from remote sensing data. *J. Geophys. Res.* **2003**, *108*, 4688-4694.
21. Sobrino, J.A.; Jimenez-Munoz, J.C.; Paolini, L. Land surface temperature retrieval from LANDSAT TM 5. *Remote Sens. Environ.* **2004**, *90*, 434-440.
22. Van de Griend, A.A.; Owe, M. On the relationship between thermal emissivity and the normalized difference vegetation index for natural surfaces. *Int. J. Remote Sens.* **2003**, *14*, 1119-1131.
23. Zhang, J.; Wang, Y.; Li, Y. A C++ program for retrieving land surface temperature from the data of Landsat TM/ETM Band 6. *Comput. Geosci.* **2006**, *32*, 1796-1805.
24. Yang, J.; Qiu, J. The empirical expressions of the relation between precipitable water and ground water vapor pressure for some areas in China. *Sci. Atmos. Sinica* **1996**, *20*, 620-626.
25. Li, J. Estimating land surface temperature from Landsat-5 TM. *Remote Sens. Technol. Appl.* **2006**, *21*, 322-326.
26. Mao, K.; Tang, H.; Chen, Z.; Qiu, Y.; Qin, Z.; Li, M. A split-window algorithm for retrieving land-surface temperature from ASTER data. *Remote Sens. Inf.* **2006**, *5*, 7-11.
27. Mao, K.; Qin, Z.; Xu, B. Method for land surface temperature from retrieval from ASTER data. *J. Inst. Surv. Mapp.* **2005**, *22*, 40-42.
28. Zhang, Y. Land surface temperature retrieval from CBERS-02 IRMSS thermal infrared data and its applications in quantitative analysis of urban heat island effect. *J. Remote Sens.* **2006**, *10*, 789-797.